BEAM
INTERACTIONS
WITH
MATERIALS
AND ATOMS

Quantitative considerations in medium energy ion scattering depth profiling analysis of nanolayers

CrossMark

P.C. Zalm [a], P. Bailey [a], M.A. Reading [b], A.K. Rossall [a], J.A. van den Berg [a],*

[a] *International Institute for Accelerator Applications, University of Huddersfield, Queensgate, Huddersfield HD1 3DH, UK*
[b] *Physics and Materials Research Centre, University of Salford, Salford M5 4WT, UK*

A B S T R A C T

The high depth resolution capability of medium energy ion scattering (MEIS) is becoming increasingly relevant to the characterisation of nanolayers in e.g. microelectronics. In this paper we examine the attainable quantitative accuracy of MEIS depth profiling. Transparent but reliable analytical calculations are used to illustrate what can ultimately be achieved for dilute impurities in a silicon matrix and the significant element-dependence of the depth scale, for instance, is illustrated this way. Furthermore, the signal intensity-to-concentration conversion and its dependence on the depth of scattering is addressed. Notably, deviations from the Rutherford scattering cross section due to screening effects resulting in a non-coulombic interaction potential and the reduction of the yield owing to neutralization of the exiting, backscattered H^+ and He^+ projectiles are evaluated. The former mainly affects the scattering off heavy target atoms while the latter is most severe for scattering off light target atoms and can be less accurately predicted. However, a pragmatic approach employing an extensive data set of measured ion fractions for both H^+ and He^+ ions scattered off a range of surfaces, allows its parameterization. This has enabled the combination of both effects, which provides essential information regarding the yield dependence both on the projectile energy and the mass of the scattering atom. Although, absolute quantification, especially when using He^+, may not always be achievable, relative quantification in which the sum of all species in a layer adds up to 100%, is generally possible. This conclusion is supported by the provision of some examples of MEIS derived depth profiles of nanolayers. Finally, the relative benefits of either using H^+ or He^+ ions are briefly considered.

1. Introduction

The ever shrinking lateral and depth dimensions of microelectronic devices have resulted in the development of viable fabrication technologies of which the functional components cannot be characterized exhaustively using any single analytical technique. Almost all techniques available are restricted to the analysis of one or more essential aspects and increasingly the prediction of the performance of a device is based on a combination of structural, compositional and electrical analysis techniques, in conjunction with simulations which are often based on measurements on model structures that circumvent the difficulties encountered with real devices.

Among the techniques that are increasingly proving their capability in this context, notably in the field of the analysis of thin films of nanometre thickness and ultra-shallow implants, is medium energy ion scattering (MEIS). Essentially a low-impact energy variant (typically 100 keV as opposed to 1 MeV) of the well-established Rutherford Backscattering Spectrometry (RBS), it enables not only precise ion crystallographic measurements [1–3], but also more importantly in the present context, quantitative depth profiling with down to sub-nanometre resolution [4–6].

The aim of this paper is to make an assessment of the attainable level of quantification in MEIS depth profiling in terms of both the depth and concentration parameters. With regards to depth, straightforward analytical calculations on a model target system will be shown to lead to a direct relationship between depth of scattering and the energy difference between ions scattered at the surface and those at greater depth. The approach used, which is also valid for complex, multi-layered compound targets, offers a clear and readily understandable insight in what can be achieved. However, in more complex layered systems, spectra can only be effectively interpreted using computer simulations that are based on the same analytical approach, but the use of simulation makes the physical basis of the approach less transparent.

* Corresponding author.
   E-mail address: j.vandenberg@hud.ac.uk (J.A. van den Berg).

As part of the quantification of atomic composition, the yield ratio of atoms scattered off the surface and those at a certain depth is compared with the Rutherford inverse energy squared prediction and the modification required is evaluated, including the effect of the dependence of the energy width of the detector channel on backscattered energy. The effect of the screening of the interaction potential on the backscattering yield in MEIS is calculated for different energies for both H$^+$ and He$^+$ ions. Although effects such as the above are typically included in various RBS and MEIS computer simulation codes currently in use, this is not necessarily the case for a correction that accounts for ions leaving the surface in a neutral state which is an effect that may become significant especially for lower energy He$^+$ ions. This correction is based on the parameterization of an extensive set of available data on surviving ion fractions. The combination of the screening and neutralization effects provides a correction factor to the Rutherford backscattering cross section ratio that enables the reliable conversion of measured ion yields to atomic concentrations to within a few % as is demonstrated in a number of representative examples of depth profiles of nanolayers derived from MEIS spectra. This leads to the conclusion that although absolute quantification, especially when using He ions, may not always be achievable, relative quantification in which the sum of all species in a layer add up to 100%, generally is. Finally, the relative benefits of either using H$^+$ or He$^+$ ions will be considered.

2. Energy loss to depth scale conversion

2.1. Monatomic target with dilute impurities

In a MEIS experiment, a well aligned beam of energetic (50–200 keV) H$^+$ or He$^+$ ions impinges on a target at an angle θ_{in} relative to the surface normal. Primary particles are backscattered at different depths and those exiting at an angle θ_{out} to the surface normal are energy-analyzed either using an electrostatic energy analyser or time of flight analysis. Toroidal electrostatic sector analysers *cum* detectors are capable of collecting a range of angles in parallel. The resulting energy or angular spectra are commonly interpreted by assuming that only a single direction-altering elastic collision has taken place and that to and from the depth where scattering took place only continuous inelastic energy losses occur. The validity of this assumption will be addressed later.

A typical characteristic of MEIS energy spectra is that each element has its own energy to depth scale conversion and differences between the various elements can be considerable. This is due to the substantial variation of the stopping power over the energy range in which MEIS operates and is illustrated in the following simple numerical example. Following [7] for the energies employed in MEIS, the stopping power at energy E can be approximated by a power law

$$-\frac{dE}{dx} = AE^B \tag{1}$$

where B is a dimensionless constant with a value not far off 0.5 for He$^+$ ions and close to 0 or even slightly negative for H$^+$ ions in this energy regime. The prefactor A is strongly material dependent and B is a fairly weak function of incident ion energy. Over an energy interval typical for MEIS applications e.g. 50–100 keV or 100–200 keV, specific material dependent constants A and B can usually be found which cause Eq. (1) to be accurate to well within 1–2%, i.e. better than the absolute accuracy of the stopping data on which it is based. This is illustrated in Fig. 1 for the stopping of He$^+$ in Si between energies of 40 and 200 keV, where the results of using Eq. (1) are compared with SRIM code calculations [8]. Therefore, in practice, there is no need for a more elaborate power expansion.
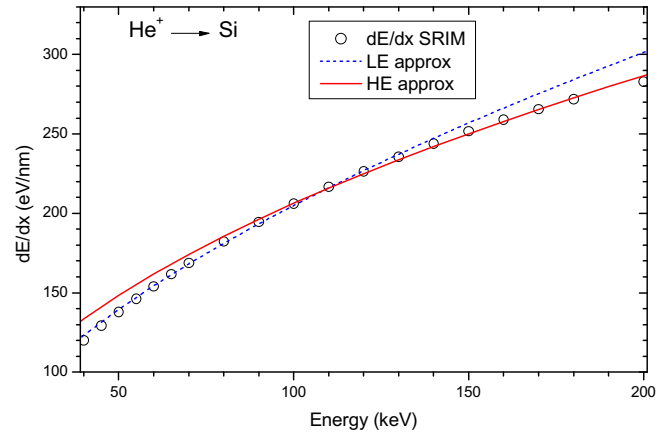

Fig. 1. SRIM calculated energy loss values in eV/nm for He$^+$ ions in Si as a function of ion energy (o). The two lines represent the approximation AE^B for low (50–100 keV) ion energy where A = 0.0143 & B = 0.58 and high (100–200 keV) ion energy where A = 0.0248 & B = 0.46 with dE/dx in keV/nm and E in keV.

The advantage of Eq. (1) is that one can solve the energy loss to depth conversion (in terms of incident particle pathlength) fully analytically [9]:

$$pathlength = \int_{E_{start}}^{E_{finish}} \frac{1}{dE/dx} dE = \frac{1}{(1-B)A}[E_{start}^{1-B} - E_{finish}^{1-B}] \tag{2}$$

We consider the rather unfavourable numerical example of 200 keV He$^+$ incident on a ^{28}Si(1 0 0) sample that contains ^{16}O and ^{76}As in the near surface layers. In the double alignment geometry where the ion beam is incident along the $[-1-1\,2]$ and backscattered particles are detected along the $[1\,1\,1]$ crystallographic direction, $\theta_{in} = 35.26°$ and $\theta_{out} = 54.74°$ and the total scattering angle is 90°. In this geometry the so-called kinematic factor, the ratio of the energy immediately after scattering to that immediately before scattering, is given by $K = (M_{target}-M_{ion})/(M_{target} + M_{ion})$.

In the energy range of 80–180 keV the approximation $-dE/dx = 0.0248E^{0.46}$ [keV/nm for E in keV] turns out to approximate the SRIM results to within 1% as shown in Fig. 1. Taking the above example and applying sequentially Eq. (2) with these constants on the way in, the kinematic factor during the collision, and Eq. (2) once again on the way out, yields an analytical relationship between depth of scattering and energy loss. Since for layer analysis purposes, an actual depth scale is generally preferred, the areal density in this calculation was converted to depth using the Si density of 5x10^{22} at/cm^3. Fig. 2 depicts the relation between $KE_{in} - E_{out}$ down to depths of 40 nm, arguably around the upper limit of what can meaningfully be probed with MEIS for the geometry and elements considered. Two things are immediately clear: (i) the near linear relationship between depth and energy and, (ii) the substantial differences between elements (the average slopes of the O and As lines differ by as much as 15% from that of Si). Note that for lower primary ion energies the scaling differences would even be larger owing to a slightly higher stopping gradient (i.e. a larger B in Eq. (1)). This is shown in Fig. 2 for 100 keV He and the same scattering geometry (stopping here has been approximated by $-dE/dx = 0.0143E^{0.58}$). For other scattering geometries the depth scale calibration could have either a weaker or a stronger dependence on element type (or M$_{target}$).

2.2. Compounds, multilayers and concentration gradients

The approximate expression of Eq. (1) is equally valid in compounds. With multi-layered samples the prefactor A is different
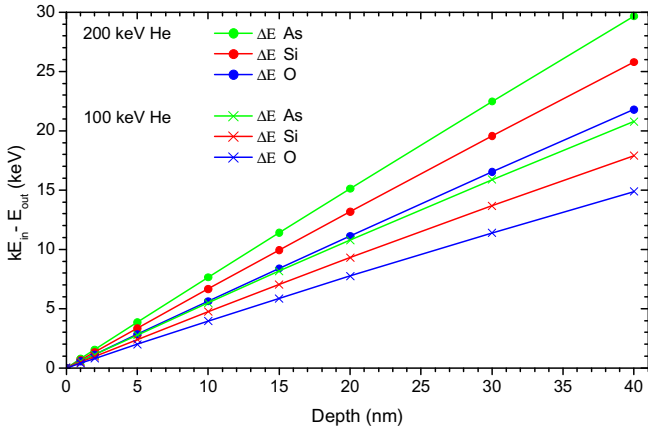
Fig. 2. Additional energy lost relative to 90° scattering off O, Si or As at the very surface (i.e. $KE_{in} - E_{out}$) as a function of the depth from which the backscattered He$^+$ ion originates, assuming E_{in} = 200 keV and θ_{in} = 36.24°, θ_{out} = 54.76° and using an energy dependent stopping power.

for each layer while B will not change significantly and the path length can no longer be calculated simply analytically. Computer simulations are needed and are commonly used in an iterative way in which the composition and areal density for each layer are assumed, the MEIS spectrum is calculated and compared with the data and the input model is adjusted accordingly.

Such simulations are carried out correctly in terms of areal densities. However any comparison with other analytical techniques or comparison with the technologist's expectations or specifications almost always requires a composition vs. depth profile and hence an estimate of the density of the individual layers. This can be quite problematic since thin layers often have a density somewhat below the bulk value. In addition, when concentration gradients are involved, due to e.g. intermixing, assumptions have to be made about the compositional dependence of the density. This may lead to severe errors even in rather straightforward cases as the following examples show.

As a first approximation it seems not unreasonable to interpret intermediate oxides of V as a mixture of metallic V and the saturated oxide V_2O_5. But in doing so one estimates the densities of the stable oxides VO, V_2O_3 and VO_2 on average over 40–20% too low and hence overestimates their thicknesses by the same amount. The situation for metals can be even worse. A most pathological example is that 1 cm^3 of gold and 1 cm^3 of caesium give 0.8 cm^3 of the 50–50 alloy AuCs. Thus it cannot be overemphasised that what is measured in MEIS is the areal density of a layer, not its thickness.

2.3. Energy straggling and discrete energy loss effects

Energy straggling poses a severe limitation on the obtainable MEIS depth resolution as it usually exceeds the energy spread of the beam or detector resolution. The resolution or response function in simulations is generally assumed to be Gaussian with a spread Ω that rises rapidly from the instrumental limit at the surface to the energy-independent Bohr estimate (see Ref. [10], $\Omega_B^2 = 0.26\ Z_i^2 Z_t\ e^2 N\ t$ (keV^2) where $N\ t$ is the "thickness" travelled in units of 10^{18} at/cm^2) as modified by Lindhard and Scharff [11] for low energy ions. All of this is based on the assumption of a continuous energy loss with depth. However, several studies have shown, both experimentally and theoretically [12–14], that the latter assumption is not realistic in the very near surface region. Here incident ions may or may not have undergone one or several discrete inelastic energy loss events in their interaction with target electrons and these losses can differ depending on the specific process involved. These energy losses result in a strongly skewed near-surface depth resolution function with an extended tail towards greater energy losses. Thus, if only a symmetric Gaussian is used to model the surface-side upslope of the peak due to a thin overlayer correctly as being almost entirely due to instrumental (or surface roughness) limitations, then pre-scattering losses are ignored. If they are incorporated by artificially introducing a broader instrumental function these would still be an underestimate at the rear- or down slope and the extended tail would not be modelled correctly. This could be corrected for by assuming some artificial, non-existent intermixing of the top and the underlying layers but then the upslope of that second layer would not fit the data properly. Suitable proposals for the asymmetric response function are given in e.g. Refs. [15,16]. The asymmetry gradually disappears with increasing depth and is approximately limited to the first 5 nm or energy losses of up to 3 keV, after which the symmetric Gaussian in the modified Bohr limit can be used.

3. Intensity to concentration conversion

3.1. Basic considerations

According to Chu et al. [9], the absolute backscattering yield off target atoms at a depth x in a homogeneous sample is given by:

$$H(E_{out}) = \sigma(E)\Omega\Phi \frac{D}{[\varepsilon(E)]cos\theta_{in}} \frac{\varepsilon(KE)}{\varepsilon(E_{out})} \qquad (3)$$

where E_{out} is the energy at the detector after scattering off a target atom at depth x, E is the energy immediately before scattering at that depth, $\sigma(E)$ the energy-dependent Rutherford scattering cross section, Ω the detector solid angle, Φ the total number of incident particles, D the detector energy bin or channel width, ε the stopping cross section (defined as $\varepsilon \equiv (1/N)(dE/dx)$, where N is the atom density [9]) and K the kinematic factor for the scattering geometry adopted. Finally, $[\varepsilon(E)]$ is called the stopping cross-section factor (9):

$$[\varepsilon(E)] = \frac{K}{cos\theta_{in}} \frac{1}{N}\frac{dE}{dx}\bigg|_E + \frac{1}{cos\theta_{out}} \frac{1}{N}\frac{dE}{dx}\bigg|_{kE} \qquad (4)$$

The term D is given as:

$$D = [\varepsilon(E)]N\tau \qquad (5)$$

where τ the thickness of the surface layer across which an ion will lose the energy equivalent to the width of a single bin within the detector.

The last term in Eq. (3), $\varepsilon(KE)/\varepsilon(E_{out})$, accounts for the fact that while the measurement of the energy of backscattered particles has a constant "error" or "width" at the detector (the channel or bin in which it is recorded), *inside* the target this no longer corresponds to a constant depth resolution as the depth increases. The reason for this is as follows: deeper inside the target the incoming particle has slowed down and consequently will experience weaker stopping (at least for He$^+$ ions below 400 keV and H$^+$ ions below 100 keV in MEIS; in RBS it may either increase or decrease depending on the position on the stopping curve). It must therefore travel greater distances at greater depth before it has lost sufficient energy to be counted in the next channel. For scattering at the top surface $E = E_0$ and $E_{out} = KE_0$ so that this final term in Eq. (3) disappears and the expression for the yield off the surface is obtained (cf. [9]):

$$H(KE_0) = \sigma(E_0)\Omega\Phi \frac{D}{[\varepsilon(E_0)]cos\theta_{in}} \qquad (6)$$

From this the change in yield due to scattering off atoms at depth x as a ratio to scattering off atoms at the surface follows directly as:

$$\frac{H(E_{out})}{(H(KE_0))} = \frac{\sigma(E)}{\sigma(E_0)} \cdot \frac{[\varepsilon(E_0)]}{[\varepsilon(E)]} \cdot \frac{\varepsilon(KE)}{\varepsilon(E_{out})} \tag{7}$$

provided the detector channel width D is independent of energy (as it usually is in RBS where solid state surface barrier detectors are employed; deviations will be discussed later). Factors like Ω, Φ and $\cos\theta_{in}$ have now dropped out of Eq. (7). Ignoring, for the moment, screening and neutralization corrections considered below, the Rutherford cross section is proportional to the inverse impact energy squared (i.e. $\sigma \propto E^{-2}$). The scattering geometry dependent stopping cross section factors $[\varepsilon]$, are defined in Eq. (4); again constants such as the atomic density are ignored in this analysis which is permissible since only ratios of either ε's or $[\varepsilon]$'s are considered here.

At this stage it becomes now immediately clear why the simple power law stopping power approximation of Eq. (1) is so particularly convenient, since:

$$\frac{[\varepsilon(E_0)]}{[\varepsilon(E)]} = \left(\frac{E_0}{E}\right)^B \quad \text{and} \quad \frac{\varepsilon(KE)}{\varepsilon(E_{out})} = \left(\frac{KE}{E_{out}}\right)^B$$

so that Eq. (7) reduces to:

$$\frac{H(E_{out})}{H(KE_0)} = \left(\frac{E_0}{E}\right)^2 \cdot \left(\frac{KE_0}{E_{out}}\right)^B \tag{8}$$

In other words, deviations from the energy dependence of the yield according to the Rutherford prediction (first term in Eq. (8)) scale with the inverse ratio of the energies *at the detector* (E_{out}) to a power $B \approx \frac{1}{2}$ (second term in Eq. (8)).

As indicated, the above discussion assumes that the detector channel width D is independent of energy. In conventional RBS analysis, in which solid state detectors are employed this is the case and Eq. (8) applies. If however D is energy dependent, Eq. (8) has to be multiplied by a ratio $D(E_{out})/D(KE_0)$. For very high resolution RBS facilities (those employing magnetic sector analysis) the transmission efficiency resembles that of e.g. an XPS instrument and is characterised by an *energy-dependence* of the form $D(E) \propto 1/E$. Under these circumstances the above correction factor would have to be multiplied by the ratio (E_{out}/KE_0). In the case of our MEIS instrument the software corrects for the detector characteristics and spectra can be compared directly against Eq. (8).

Evaluating Eq. (8) with the help of Eq. (2) reveals that the yield rises with increasing depth at a rate of less than one percent per nanometre depth. For the example of Section 2.1 the depth to surface yield ratio $H(x)/H(0) \approx 1 + 0.0055x$. The slope varies somewhat with scattering geometry but is almost independent of the target element. The reason for the latter is that the ratio $\sigma(E)/\sigma(E_0)$ is the same for all elements at any given depth. The same holds for $[\varepsilon(E_0)]/[\varepsilon(E)]$. Only the term $\varepsilon(KE)/\varepsilon(E_{out})$ will change with depth, but it will do so very weakly.

A final comment to be made is that Eq. (8) is equally valid for multi-layered samples because it combines the ratio $[\varepsilon]/\varepsilon$, evaluated at the surface with its inverse evaluated at some arbitrary depth. But in each of these ratios, the material-dependent prefactor A governing the magnitude of the energy loss (cf. Eq. (1)) cancels and as argued before, B predominantly depends on the incident ion energy and hardly at all on the material type.

3.2. Screening correction

In the foregoing it has been assumed that the Rutherford scattering cross section is exactly valid. Whilst this is correct at the high projectile energies employed in RBS (~2 MeV), in MEIS, partial

screening of the scattering centres by the surrounding electron cloud cannot be ignored. Various authors [17–19] have addressed this issue. To estimate the magnitude of the effect the approach of Andersen et al. [19] is followed which was found to agree well with exact classical calculations using Dirac–Fock atomic potentials [20]. Their starting point is the screened Coulomb potential:

$$V(r) = \frac{Z_i Z_t e^2}{r} \varphi\left(\frac{r}{a}\right) \tag{9}$$

Here Z_i and Z_t are the atomic numbers of the projectile and target particles used, respectively, $\varphi(r/a)$ is the so-called screening function and a, the screening length that depends on the atomic numbers of the colliding particles. At $r = 0$, $\varphi = 1$ which gives the unscreened Coulomb potential. Expanding φ near $r = 0$ to first order in a Taylor series yields:

$$\varphi\left(\frac{r}{a}\right) \approx 1 + \frac{r}{a}\dot{\varphi}(0) \tag{10}$$

with $\dot{\varphi}(0)$ the gradient of the screening function at the origin. Inserting Eq. (10) into Eq. (9) leads to:

$$V(r) = \frac{Z_i Z_t e^2}{r} + \frac{Z_i Z_t e^2}{a}\dot{\varphi}(0) = V_{coulomb} + V_{const} \tag{11}$$

Thus, because $\dot{\varphi}(0)$ is negative, to first order the effect of screening is to *decrease* the Coulomb potential by a constant amount. Andersen et al. [19] incorporated this by *increasing* the kinetic energy of the projectile in the center-of-mass system by exactly the same amount. By doing this, the unscreened potential can still be used, only E is replaced by $E + V_{const}$ in the Rutherford cross section. The net effect is to decrease the scattering cross section progressively with increasing atomic number of the target nucleus. It should be mentioned that the Andersen correction is only valid for scattering angles larger than, say 60° [19], but smaller angles are not normally used in MEIS.

The effect of screening has been evaluated for scattering off the outermost surface layer of targets ranging from C to Bi, for both H^+ and He^+ ions at incident energies of 50, 100 and 200 keV. A number of scattering angles commonly used in MEIS (viz. 125.26°, 90°, 70.5° and 60.5°) have also been considered. Different proposals for the screening function $\varphi(r/a)$ in Eq. (9) have been tried for the evaluation of V_{const}, for instance the one by Lenz-Jensen (LJ) as suggested in Ref. [19], or that of Molière [21] and, finally, the universal potential of Biersack and Ziegler (BZ) [22]. As the screening corrections for the Molière potential were found to fall in between the estimates from the other two interaction potentials they are not discussed any further. Fig. 3 shows the screening correction factor P_{scr} as a function of the target atomic number, for 100 keV He^+ at three scattering angles using the BZ potential. In addition, the results for 90° scattering at a depth of 40 nm in Si (same potential) and off the surface but now using the LJ potential are included in the figure. Finally, the result for 50 keV H^+ ions, again with the BZ potential and 90° scattering is also shown in the figure.

A number of conclusions can be drawn from this set of calculations and be understood in a surprisingly straightforward way. Following Andersen [19] and ignoring the center-of–mass aspect, one can write the screening correction factor P_{scr} approximately as:

$$P_{scr} \equiv \frac{\sigma(E_0 + V_{const})}{\sigma(E_0)} = \left(1 + \frac{V_{const}}{E_0}\right)^{-2} \approx 1 - f\frac{Z_1 Z_t}{E_0} \tag{12}$$

Here f has a near constant value that depends almost entirely on the expression for the potential adopted and is only weakly dependent on the other parameters, Z_1, Z_t and Θ. Indeed Fig. 3 shows in all cases an almost linear dependence on Z_t and an intercept (for a hypothetical $Z_t = 0$), $P_{scr} = 1 \pm 0.015$. Furthermore, a constant ratio Z_i/E_0 (e.g. 50 keV H^+ or 100 keV He^+) gives nearly the same result, as shown. The scattering geometry plays a minor role albeit that
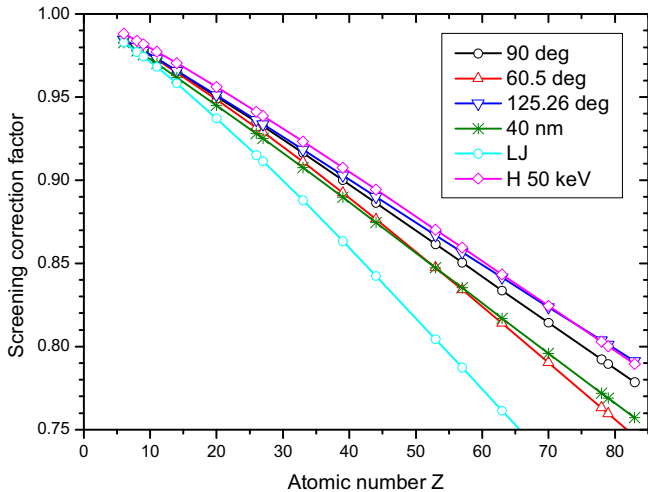
Fig. 3. Absolute screening correction to the yield of 100 keV He$^+$ ions backscattered at different scattering angles (125.26°, 90° and 60.5°) as a function of the target atomic number. The Biersack-Ziegler universal interatomic potential (see text) was used in the evaluation. Also included in the graph for 90° scattering are: the screening corrections for He$^+$ ions scattered at a depth (40 nm), for 50 keV H$^+$ ions (H 50 keV) and when using a Lenz Jensen (LJ) potential.

the corrections, as is to be expected, become somewhat larger for small angle collisions as compared to large angle, high energy transfer ones. This is illustrated in Fig. 3 by the 60.5° result compared to that for 125.26°. A different form for the interatomic potential, however, such as the Lenz Jensen (LJ), may give rise to considerable (25%) variation in the slope of f and thereby introduce substantial uncertainty in the magnitude of the screening correction to be applied. This in turn affects the calculation of the concentration of heavy atoms as is illustrated by the LJ result for He shown in the figure. It is also clear that compared to that uncertainty, the additional systematic errors introduced by applying the screening correction, evaluated at the surface, but applied at all other attainable depths can be safely ignored as demonstrated by the result for He$^+$ scattered at 90° from a depth of 40 nm. For a good first order estimate we may set f = 0.16 [keV] in Eq. (12) with a 25% error (or ±0.04) to estimate the intrinsic uncertainty by evaluating the screening correction, which is applicable to all situations investigated here.

3.3. Neutralization correction

Until now it has also been assumed that the detection efficiency is independent of the scattered ion energy. This is certainly correct in RBS when employing solid state, surface barrier detectors that detect ions and neutrals with the same efficiency and remains approximately valid when energy analysis in a magnetic sector is used because of the high projectile velocities. However, in MEIS systems employing an electrostatic sector analyzer, only charged particles of comparatively moderate velocity are analyzed and for that reason a degree of neutralization of scattered particles when leaving the sample, can no longer be ignored. This is not case for modern TOF-MEIS instruments [23,24] which do not suffer from this problem.

Ion survival probabilities are not very accurately known. The FOM group, who may be considered as the founding fathers of the MEIS technique, collected a substantial data library ($\geqslant$50 sets) of ion survival fractions for H$^+$ impact on more than 10 different target materials including metals and semiconductors in the energy range 50–175 keV and a more limited dataset for He$^+$ [25]. These data taken at 5 different energies for H$^+$ and 2 energies

for He$^+$ are shown averaged in Fig. 4. The data point for 100 keV H$^+$, for example, is the result of more than 30 closely spaced measurements. Busch [26] also reported on H$^+$ ion beams and these results are included in the figure (Rutgers). The FOM data augmented by results obtained by Kim et al. [27] suggests that there is little to no dependence on target atom or scattering geometry for either H$^+$ or He$^+$, albeit that, as mentioned, the data for He$^+$ is limited. On the other hand, Kitsudo et al. [28] did observe variations with target atom type for He$^+$ but not for H$^+$ as demonstrated by their results for some metal and semiconductor surfaces which are also shown in Fig. 4. They also observed a dependence on emergence angle for metal surfaces and similarly Kido [29] observed angular variations on very clean surfaces. Nonetheless, based on available data a general form for the ion survival probability may be expressed as [25]:

$$P_{ion} = 1 - e^{-\alpha E} \qquad (13)$$

where E is the projectile energy upon exit from the surface and α a projectile dependent constant. Eq. (13) with a value for α = 0.019 keV^{-1} for H is found to agree well with all available FOM data and sensibly reaches the value 1 for high energies (curve marked H Eq. (13)). For energies below 100 keV the results of Kitsudo also match this curve as shown in Fig. 4. However the apparent saturation of these data to an ion fraction of $\sim$0.85 for energies above 100 keV is difficult to rationalize. For He$^+$ ions a value α = 0.0064 keV^{-1} matches the available FOM data (including the zero point) and also the results found by Kitsudo for Si, SiO$_2$ and HOPG, albeit not for metals. Importantly, as will be shown in Section 4, the ion fraction values, given by the curve marked He Eq. (13), results in a quantitatively reliable compositional characterization of several compound targets, collected in different scattering geometries using the MEIS technique. Other, target-independent, proposals for the ion survival fraction P_{ion} such as e.g. by Marion and Young [30], derived from expressions for the average charge state in solids (i.e. $P_{ion} = 1 - e^{-\alpha v}$, with v the exiting ion velocity and α again a constant, cf. [31,32]) agree less well with the available data as is again shown in Fig. 4. Hence we adopt Eq. (13) for He$^+$ as well as H$^+$. It must be borne in mind however, that in view of the results of Kitsudo, the use of Eq. (13) for He$^+$ scattering, under certain conditions, could be out by as much as 50% in an absolute sense
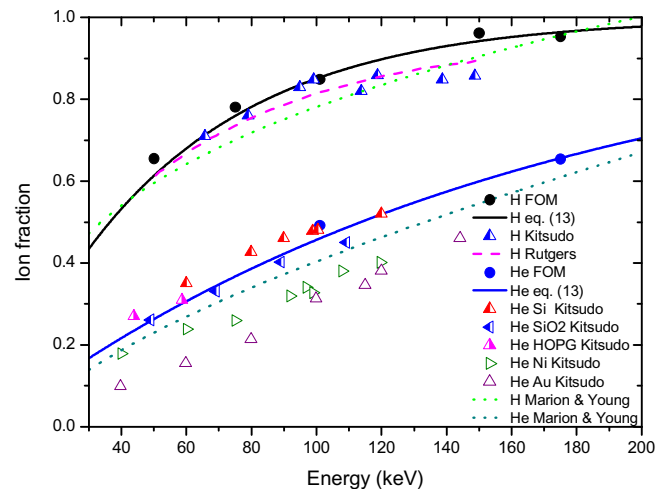

Fig. 4. Ion fractions data for H$^+$ and He$^+$ ions scattered a wide range of surfaces as a function of exit energy measured at the FOM lab (solid circles) [25], by Kitsudo et al. [28] (triangles) and by the Rutgers group [26] for H$^+$ ions (dashed line). Solid curves are given by Eq. (13) (parameter values in the text) and the results of Marion and Young [30] are represented by dotted lines.

below 150 keV. However, when concentrations within a layer are summed to 100%, relative errors will clearly be substantially less.

Regardless of the exact form of the primary ion survival probability P_{ion}, it is clear that the effect of this factor on the signal intensity is greatest for scattering off lighter target atoms. This is shown in Fig. 5 where Eq. (13) is evaluated as a function of target atom number for both H^+ and He^+ ions scattered at energies of 50, 100 and 200 keV through 90°. As shown above, the effect of screening is strongest for higher atomic numbers (Fig. 3) and there is only minor cancelling out due to screening as the two effects dominate at opposite ends of the atomic number scale. To facilitate comparison, all curves in Fig. 5 were normalized to the theoretical maximum, i.e. $P_{ion}(E_0)$. The analysis presented in Fig. 5 implies that the interpretation of MEIS ion spectra to obtain *absolute* quantitative data on the target composition is generally not feasible and it is only possible to achieve a *relative* quantification in which the sum of all concentrations at a given depth adds up to 100 at%. Essentially, the necessary corrections are considered to be most reliable on a relative scale.

What is apparent from Fig. 5 is that when H^+ projectiles are used the corrections are always comparatively minor and very much restricted to scattering off the lowest identifiable masses (roughly C, F) whereas for He^+ they already become significant for the whole lower half of the stable elements in the periodic table. The figure also shows the result for 100 keV He^+ scattered at a depth of 40 nm in Si, normalized to that valid for scattering off the surface (40 nm surf), illustrating that scattering at this rather extreme depth in Si reduces the values of P_{ion} significantly relative to those for scattering off the surface. Inspection however shows that this is a reduction with nearly a constant factor. What is clear however, is that this correction needs to be evaluated properly at each depth.

It is instructive to consider the combination of both the screening and neutralization corrections presented in Figs. 3 and 5 as a function of the atomic number of the analyzed species. This leads to a correction curve for the Rutherford cross section ratio between a specific species analyzed (e.g. O, As or Hf, etc.) and the bulk material (Si). Calculated correction curves for He^+ incident at energies of 50, 100 and 200 keV and scattered through 90° off Si (e.g. $[-1-11]$ in, $[112]$ out) are shown in Fig. 6 as a function of the atomic number. They illustrate that this correction is both mass and energy
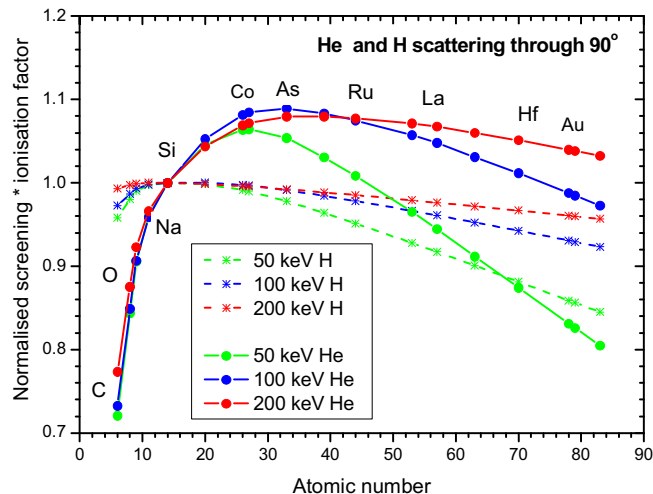

Fig. 6. Combined screening and neutralization corrections to the Rutherford cross section for 90° scattering of either He^+ (full) and H^+ (dashed) at 50, 100 and 200 keV as a function of target atom number. Normalization to the correction value for Si was applied in all cases. The Biersack-Ziegler universal potential and exponentially energy dependent ion survival (Eq. (9) in the text) were used in the calculations.

dependent, as expected since the energy after scattering depends on the target atomic mass. As discussed above, neutralization has its strongest effect on the ion yields for scattering off low masses (resulting in low exit energies and reduced degree of ionization) whereas for scattering off higher masses (e.g. Hf, Au), where the interpenetration of the electron clouds during scattering is incomplete, the screening correction has the stronger influence. The combined effects of these corrections only cancel each other to some degree for atomic masses in the medium range of atomic numbers. For the conditions considered, the combined correction factors cause a change in ion yield of +3% and −15% for 100 keV He^+ scattered through 90° off Hf and O, respectively, as referenced to Si, increasing to −21% for N, both in comparison to the Rutherford cross section ratio. Clearly, corrections such as these needs to be taken into account when trying to extract quantitative data from MEIS spectra.

4. Experimental confirmation

In the previous section it was shown that whereas the effects of screening can be handled fairly precisely, the effects of neutralization are potentially more severe for lighter target atoms when attempting quantification of MEIS depth profiles collected employing He^+ scattering and detection. In the following examples, however, we will demonstrate that in practice the combined application of Eq. (13) and the screening correction Eq. (12) works remarkably well in very different situations in spite of the limited experimental data on ion fractions available for He^+. These examples are taken from previous studies [6,33] where they have been discussed in more detail. In this section only aspects relevant to the quantification of ion yield and layer depths are discussed and only briefly. In all cases the experimental MEIS spectra were fitted using a spectrum simulation code [34], that operates within the IGOR©6 graphing software [35]. A brief description of the simulation model is given in [33]. It should be mentioned that the screening and ion fraction corrections for H^+ or He^+ presented in Section 3 are fully implemented in the model. The model outputs are the fitted MEIS spectra and the corresponding best fit depth profiles of the species present in the layer. With regards to the results for the depth scale and layer thickness presented, it is clear that the
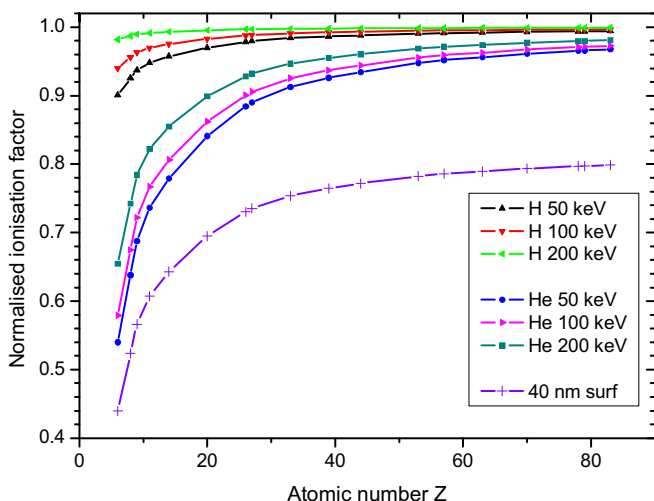

Fig. 5. Normalized ion probability for 50, 100 and 200 keV H^+ or He^+ ions scattered off the surface over 90° as a function of target atom number. Also shown is the result for 100 keV He^+ scattered at a depth of 40 nm in Si, normalized to that value for scattering off the surface (40 nm surf).

accuracy of these depend crucially on the correct values of the layer density and stopping powers. Although in the examples given below SRIM calculated values have been used these are not necessarily the most accurate available [39].

Example 1 concerns the MEIS analysis using 100 keV He$^+$ scattered through 90° off a nominally 3 nm thick TiN layer on Si (1 0 0) as typically used in a microelectronics metal/ insulator/ metal capacitor (MIM cap) layer. In this case the ion beam was aligned with the [−1 −1 1] channel and the analysis was performed along the [1 1 2] crystallographic direction. The MEIS spectrum obtained is shown in Fig. 7a with the different scattering peaks annotated and the best fit depth profiles show the atomic fraction as a function of depth in Fig. 7b. Note that the Si dechanneling background was fitted and subtracted before performing the simulation. In all examples presented here the given, nominal layer structure is indicated within the depth profile figure. Using the bulk density the thickness of the TiN layer, determined by the half heights of the Ti and N profile downslopes, is found to be 2.6 nm, more than 10% below the nominal value. This is not unexpected since the thin film density is often observed to be ~10–15% below the bulk value [36,37]. A narrow O peak showing the presence of a thin (~0.6 nm) surface oxide is due to reoxidation of the nitride layer. Away from the surface oxide the Ti and N profiles coincide, indicating that TiN layer is stoichiometric and demonstrating that the ~20% difference between the two combined correction factors for the two species, is correctly accounted for. In passing, it should be mentioned that in this and the following examples, the Si peak, because of the double alignment conditions, never reaches the Si scattering height recorded for a random Si sample.
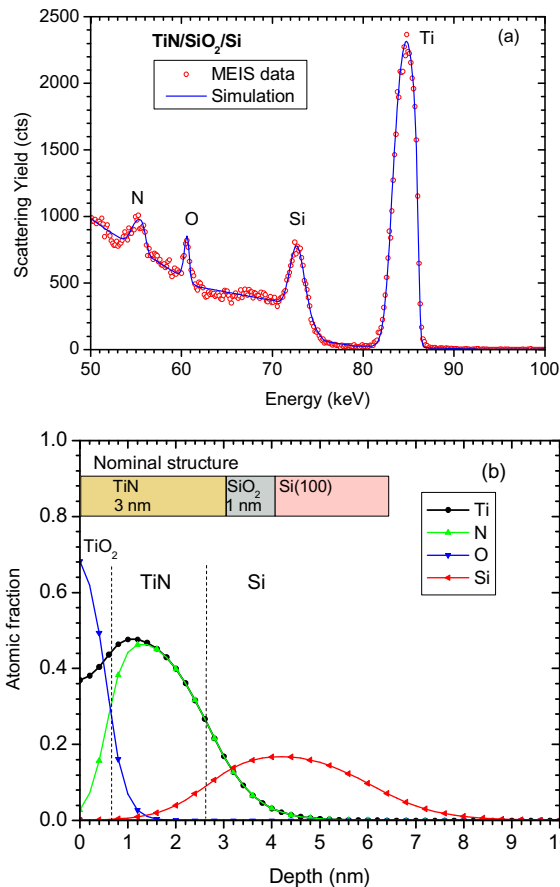
In the second example, a strontium rich titanate (STO) thin layer, a dielectric considered for MIMcap dielectric applications, was added to the above TiN layer. MEIS analysis was performed using the scattering conditions used in example 1 [33]. The energy spectrum and best fit simulation are presented in Fig. 8a and the corresponding depth profiles in Fig. 8b which again includes the structure of the layer. Note that the Si peak, lying below the STO layer was not included in the simulation. Using a STO density of 85% of the bulk value as determined by Menou et al. [37] the thickness of the STO layer is determined to be 3.3 nm and that of the TIN layer 2.9 nm, in both cases close to the nominal values. Focusing on the composition of the top STO layer, the Ti in this layer is represented by the high energy shoulder on the Ti peak at ~83 keV. The very sharp high energy edge of the Sr peak indicates surface Sr enrichment as discussed in [33]. For this reason the measurement of the relative Sr/Ti composition in this STO layer is taken in the middle of the layer, away from the enriched near surface region. It yields the value $Sr/(Sr + Ti) = 0.6$ which compares well with an RBS measurement of 0.62 [33] and confirms the appropriateness of the corrections applied in the model.

Example 3 relates to a nominally 2 nm thick high-K HfO$_2$ layer deposited on top of a 1 nm thick SiO$_2$ layer on Si(1 0 0). MEIS spectra using 100 keV He$^+$ scattering through 70.5° ([−1 −1 1] in, [1 1 1] out, double alignment conditions) as well as best fit depth profiles obtained using the bulk density of 9.7 g cm^{-3} for HfO$_2$ [33] are shown in Fig. 9a and b, respectively. The derived HfO$_2$ layer thickness is 1.6 nm, but because of the reduced thin film density already referred to [36], this may be closer to 1.75 nm, still less than the nominal value. It should be noted that alternative techniques
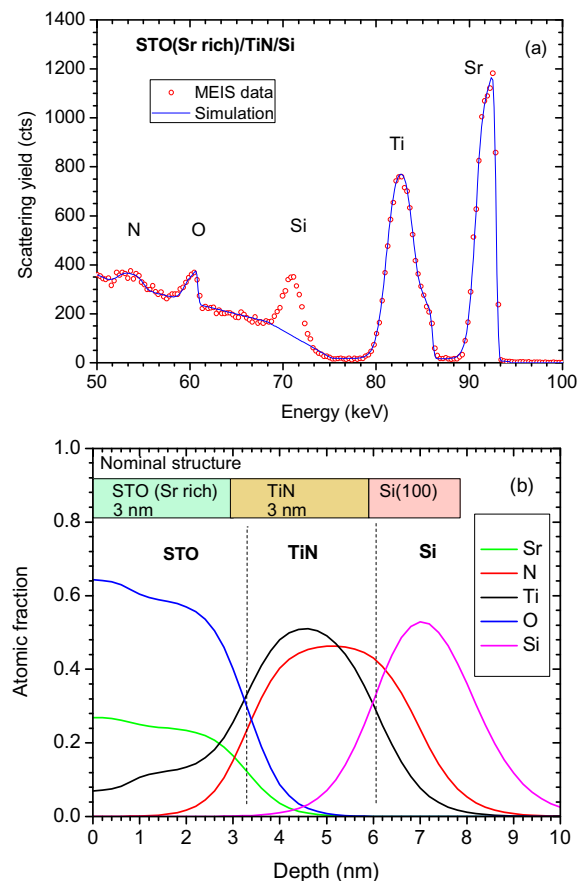

Fig. 7. (a) MEIS energy spectra and model simulations and (b) simulated best fit depth profiles for the TiN/SiO$_2$/Si layer structure shown.

Fig. 8. (a) MEIS energy spectra and model simulations and (b) simulated best fit depth profiles for the STO(Sr rich)/TiN/Si layer structure as shown.
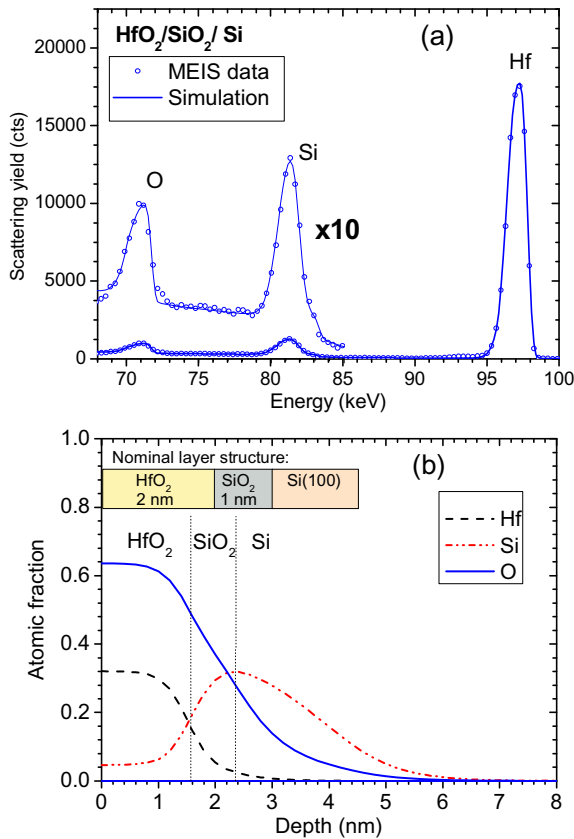
Fig. 9. (a) Energy spectra and model simulations and (b) derived best fit depth profiles for the HfO$_2$/SiO$_2$/Si layer structure indicated.

Fig. 10. (a) Energy spectra and model simulations and (b) derived best fit depth profiles for the Hf$_{0.6}$ Si$_{0.4}$O$_2$/SiO$_2$/Si layer structure indicated.

confirm the MEIS result [38]. Significantly, the HfO$_2$ layer is found to be stoichiometric to within a few % and, interestingly, is observed to have a ~5% Si content.

In the final example the HfO$_2$ layer in the above example was replaced by a Hf$_{0.6}$Si$_{0.4}$O$_2$ layer. The MEIS spectrum of this layer structure is shown in Fig. 10a. The best fit depth profiles are given in Fig. 10b and for this case Bragg's rule was used to calculate the electronic stopping rates. The density used in the calculations was 6.7 g cm^{-3} and the resulting Hf silicate thickness arrived at was 1.4 nm. As in example 2, a 10% lower density would yield a layer thickness of ~1.6 nm, which is still below the nominal value of 2 nm. Importantly though, the simulation shows that the Hf silicate analyzed has the as grown Hf/Si ratio of 0.6/0.4 to within a few %.

Concluding this section, the examples presented show that the ion survival and screening corrections work well and result in the correct ratio of species in a layer despite deviations of up to 20% from the Rutherford backscattering. It has to be mentioned that on occasions deviations do occur, especially when applying the normalization of the top layer to deeper layers and this reinforces the statement made in Section 3.2 that normalization and hence quantification, should be made within each layer.

5. Projectile considerations: He$^+$ or H$^+$

In view of the lower margin of uncertainty in the yield quantification when using H$^+$ ions in MEIS, as discussed in Section 3, a comment about the benefits of using He$^+$ ions is appropriate. The use of He$^+$ ions has the benefit of an increase of a factor 4 in the cross section for scattering compared to H$^+$, albeit that the benefit
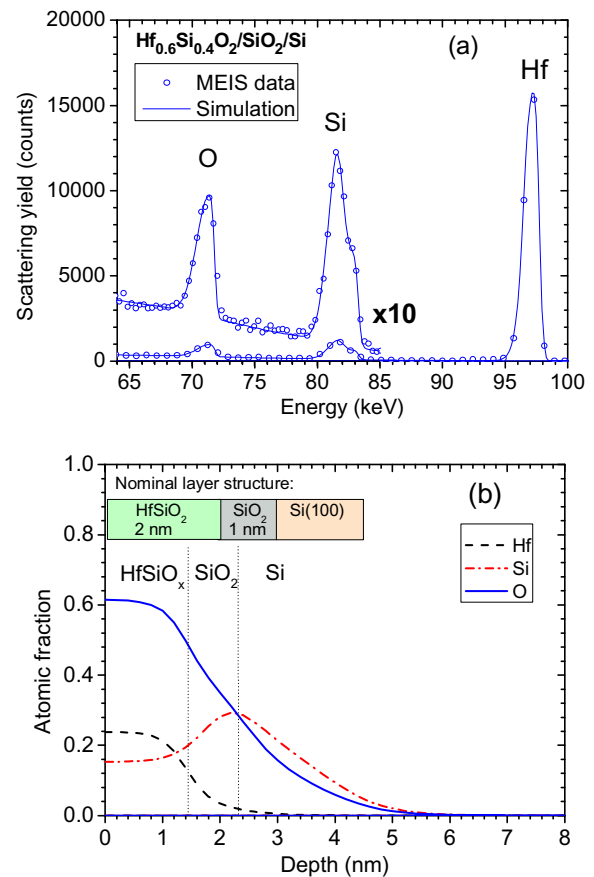
is somewhat reduced due to the increased neutralization. Nonetheless the net gain is real. The concern about increased target damage rates when using He$^+$ ions can be dealt with by moving the target normal to the plane of scattering during analysis, thus ensuring a "fresh" surface during the overall collection of the complete spectrum. This approach was introduced at Daresbury Laboratory and continues to be used in the IIAA MEIS set up. A second clear advantage is the improved mass resolution using He$^+$ ions. Additional benefit is draw from the higher inelastic loss rates for He compared to H ions which (in principle) lead to a higher depth resolution. These advantages also apply to TOF-MEIS systems, where neutralization is no longer a source of uncertainty. A final consideration in favour of using He$^+$ beams relates to the practical aspects of greater ease of ion beam operation, beam reliability and of higher He$^+$ ion current drawn from the duoplasmatron ion source used in our setup, typically by a factor 10. These are factors that become increasingly important when data acquisition times for a full 2 D spectrum, extend to something of the order of 1 h. Finally, there are the experimental results presented above that confirm that using He$^+$ ions in different scattering geometries, after evaluation of the combined correction for the screening (following the Andersen approach and using the Biersack-Ziegler potential) and neutralization (employing Eq. (13) at the appropriate energy) produces the correct stoichiometry or species ratios on a diverse range of targets such as TiN, STO/TiN, HfO$_2$ and HfSiO$_2$ nanolayers. Taken together these considerations fully justify the use of He$^+$ ions in the majority of depth profiling applications, despite the somewhat increased uncertainty in the stopping powers for He as compared to H which, of course, primarily affects the accuracy of measurement of the thickness of a nanolayer.

6. Conclusions

The level of quantification achievable in MEIS depth profiling both in terms of depth and yield has been investigated. The application of straightforward, analytical calculations on a model target system (pure silicon with dilute impurities) has shown not only the linear relationship between the depth of scattering and the energy difference between scattering off a surface atom and off one at greater depth but, importantly, demonstrated the strong dependence of the depth scale on the mass of the target atom. Although the situation for multi-layered or compound targets is more complicated, this simple approach offers an elegant demonstration of what can be achieved. MEIS spectra of these more complex targets can only be interpreted with computer simulations, that basically do more of the same but in a less transparent way.

In terms of the quantification of atomic composition, the yield ratio of particles scattered off surface atoms and those at greater depth in MEIS has been analyzed which has led to a modification of the Rutherford E^{-2} prediction by the inverse ratio of the energies of the particles arriving at the detector. The dependence of the energy width of the detector channel on the energy has also been assessed. The impact of screening of the repulsive potential on the backscattering yield in MEIS has been evaluated for different energies for both H$^+$ and He$^+$ ions using the Andersen screening correction. Furthermore, the effect of neutralization of backscattered ions which becomes not negligible, especially for He$^+$ ions, has been considered. Its magnitude has been evaluated by making use of a data set of ion fractions for both H$^+$ and He$^+$ ions scattered off various surfaces. Its parameterization and combination with the screening effect has been shown to lead to a correction factor to the Rutherford backscattering cross section ratio, the dependence of which on both projectile energy and the mass of the scattering atom is presented. The validity of this approach has been demonstrated for a number of representative examples of MEIS spectra derived depth profiles of nanolayers. This has led to the conclusion that although absolute quantification especially when using He ions, may not always be achievable, relative quantification in which the sum of all species in a layer add up to 100%, generally is. Finally, relative benefits of either using H or He ions have been discussed.

Acknowledgements

References

[1] J.F. van der Veen, Surf. Sci. Rep. 5/6 (1985).
[2] R.M. Tromp, Practical surface analysis, in: D. Briggs, P. Seah (Eds.), Ion and Neutral Spectroscopy, second ed., vol. 2, John Wiley Ltd., New York, 1992, Medium Energy Ion Scattering.
[3] P. Bailey, T.C.Q. Noakes, P. Woodruff, Surf. Sci. 426 (1999) 358.
[4] T. Gustafsson, H.C. Lu, B.W. Busch, W.H. Schulte, E. Garfunkel, Nucl. Instr. Meth. Phys. Res. Sect. B 183 (2001) 146.
[5] M. Werner, J.A. van den Berg, D.G. Armour, W. Vandervorst, E.H.J. Collart, R.D. Goldberg, P. Bailey, T.C.Q. Noakes, Nucl. Instr. Meth. Phys. Res. B 216 (2004) 67–74.
[6] M.A. Reading, J.A. van den Berg, P.C. Zalm, D.G. Armour, P. Bailey, T.C.Q. Noakes A. Parisini, T. Conard, S. De Gendt, J. Vacuum Sci. Technol., B 28 (2010) C1–C65.
[7] R. Berisch, B.M.U. Scherzer, Thin Solid Films 19 (1973) 247.
[8] J.F. Ziegler, J.P. Biersack, U. Littmark, The Stopping and Range of Ions in Solids, Pergamon, New York, 1985, http://srim.org/.
[9] W.K. Chu, J.W. Mayer, M. Nicolet, Backscattering Spectrometry, Academic, New York, 1978.
[10] N. Bohr, Mat. Fys. Medd. Dan. Vid. Selsk. 24 (1948) 19.
[11] J. Lindhard, M. Scharff, Mat. Fys. Medd. Dan. Vid. Selsk. 27 (1953) 1.
[12] W.H. Schulte, B.W. Busch, E. Garfunkel, T. Gustafsson, G. Schiwietz, P.L. Grande, Nucl. Instr. Meth. B183 (2001) 16.
[13] P.L. Grande, A. Hentz, G. Schiwietz, W.H. Schulte, B.W. Busch, D. Starodub, T. Gustafsson, Phys. Rev. B 69 (2004) 104112.
[14] M.A. Munoz-Marquez, G.S. Parkinson, D.P. Woodruff, A. Hentz, P.L. Grande, G. Schiwietz, T.J. Wood, C. Bonet, S.P. Tear, P. Bailey, T.C.Q. Noakes, Phys. Rev. B 72 (2005) 075415.
[15] P.L. Grande, A. Hentz, R.P. Pezzi, I.J.R. Baumvol, G. Schiwietz, Nucl. Instr. Meth. Phys. Res. B 256 (2007) 92.
[16] A.P. Pezzi, C. Krug, P.L. Grande, E.B.O. da Rosa, G. Schiwietz, L.J.R. Baumvol, Appl. Phys. Lett. 92 (2008) 164102.
[17] J. L'Ecuyer, J.A. Davies, N. Matsunami, Nucl. Instr. Meth. 160 (1979) 337.
[18] M. Hautala, M. Luomajärvi, Rad. Effects 45 (1980) 159.
[19] H.H. Andersen et al., Phys. Rev. A 21 (1980) 1891.
[20] S.R. Lee, R.R. Hart, Nucl. Instr. Meth. Phys. Res. B 79 (1993) 463.
[21] G. Moliere, Z. Naturforsch. 29 (1947) 133.
[22] J.P. Biersack, J.F. Ziegler. in: Ion Implantation Techniques H. Ryssel, H. Glawischnig, (Eds.), Springer, Heidelberg 1982.
[23] M.K. Linnarsson, A. Hallen, J. Åström, D. Primetzhofer, S. Legendre, G. Possnert, Rev. Sci. Instrum. 83 (2012) 095107.
[24] T. Kobayashi, Phys. Rev. B 75 (2007) 125401.
[25] P. Bailey, unpublished data.
[26] B.W. Busch, Doctor Thesis, Rutgers University, (2000).
[27] J. Kim, W.N. Lennard, C.P. McNorgan, J. Hendriks, I.V. Mitchell, D. Landheer, J. Gredley, Curr. Appl. Phys. 3 (2003) 75.
[28] Y. Kitsudo, K. Shibuya, T. Nishimura, Y. Hoshino, I. Vickridge, Y. Kido, Nucl. Instr. Meth. B 267 (2009) 566.
[29] Y. Kido, T. Nishimura, Y. Hoshino, E. Toyoda, T. Nakada, Phys. Rev. B 64 (2001) 193403.
[30] J.B. Marion, F.C. Young, Nuclear Reaction Analysis, North-Holland Publishing Co., Amsterdam, 1968.
[31] H.D. Betz, Rev. Mod. Phys. 44 (1972) 46.
[32] J.D. Garcia, R.J. Fortner, T.M. Kavanagh, Rev. Mod. Phys. 45 (1973) 111.
[33] J.A. van den Berg, M.A. Reading, P. Bailey, T.Q.C. Noakes, C. Adelmann, M. Popovici, H. Tielens, T. Conard, S. de Gendt, S. van Elshocht, Appl. Surf. Sci. 281 (2013) 8–16.
[34] P. Bailey, to be published.
[35] IGOR© Pro, Wavemetrics (http://www.wavemetrics.com).
[36] S. Bernardini, M. MacKenzie, O. Buiu, P. Bailey, T.C.Q. Noakes, W.M. Davey, B. Hamilton, S. Hall, Thin Solid Films 517 (2008) 459.
[37] N. Menou et al., J. Appl. Phys. 106 (2009) 094101.
[38] J.A. van den Berg et al., ECS Transact 25 (3) (2009) 349–361.
[39] K. Wittmaack, Nucl. Instr. Meth. Phys. Res. B 380 (2016) 57–70.